Atmos. Chem. Phys., 25, 12037–12049, 2025
https://doi.org/10.5194/acp-25-12037-2025

Atmospheric Chemistry and Physics
Open Access
EGU

Measurement report: simultaneous measurement on gas- and particle-phase water-soluble organics in Shanghai: enhanced light absorption of transported Asian dust

Zheng Li[1], Gehui Wang[1,2], Binyu Xiao[1], Rongjie Li[1], Can Wu[1,2], Shaojun Lv[1], Feng Wu[3], Qingyan Fu[4], and Yusen Duan[5]

[1]Key Lab of Geographic Information Science of the Ministry of Education, School of Geographic Sciences, East China Normal University, Shanghai 210062, China
[2]Institute of Eco-Chongming, 20 Cuiniao Rd., Chongming, Shanghai 202150, China
[3]State Key Laboratory of Loess and Quaternary Geology, Institute of Earth Environment, Chinese Academy of Science, Xi'an 710061, China
[4]Key Laboratory of Formation and Prevention of Urban Air Pollution Complex, Ministry of Ecology and Environment, Shanghai Academy of Environmental Sciences, Shanghai, 200233, China
[5]Shanghai Technology Center for Reduction of Pollution and Carbon Emissions, Shanghai, 200233, China

Correspondence: Gehui Wang (ghwang@geo.ecnu.edu.cn) and Can Wu (cwu@geo.ecnu.edu.cn)

Received: 13 February 2025 – Discussion started: 20 March 2025
Revised: 25 July 2025 – Accepted: 13 August 2025 – Published: 2 October 2025

Abstract. To better understand the physicochemical evolution of Asian dust particles during long-range transport, water-soluble organic compounds (WSOCs) in gas- ($WSOC_g$) and particle-phase ($WSOC_p$) in the spring atmosphere of Shanghai during the 2023 dust storm period (DS) and haze events (HE) were simultaneously measured with a 3 h time resolution, and characterized for their optical properties and size distribution. Our results showed that gas-to-particle-phase partitioning coefficients (F_p) of WSOCs in DS (0.30 ± 0.06) was comparable to that in HE (0.32 ± 0.06), although both temperature and relative humidity in DS were not favorable for the partitioning, indicating a promoting role of dust particles in the transformation process of $WSOC_g$ from gas to particle phase. F_p variation was largely driven by aerosol liquid water content in HE but by aerosol acidity in DS. $WSOC_p$ and its light absorption at $\lambda_{365\,nm}$ dominated at the fine mode (< 2.1 µm) in non-DS period and the coarse mode (> 2.1 µm) in DS, respectively. Mass absorption coefficient (MAC) of the coarse mode of $WSOC_p$ at $\lambda_{365\,nm}$ in DS was $0.8\,m^2\,g^{-1}$, which is four times that ($0.20 \pm 0.09\,m^2\,g^{-1}$) in the source region of Tengger Desert, suggesting a remarkably increase in light absorbing ability of Asian dust during long-range transport. Sharp co-increases of nitroaromatics, imidazoles, and water-soluble organic nitrogen at the coarse mode in the DS period further revealed that such an increasing MAC is mainly caused by adsorption and heterogeneous formation of light absorbing nitrogen-containing organics on the dust surface during long-range transport.

Published by Copernicus Publications on behalf of the European Geosciences Union.

1 Introduction

Dust storm (DS) release up to 2 billion tons of dust particles into the global atmosphere annually, exerting significant impacts on visibility, climate, and ecological environment (Li et al., 2014; Tang et al., 2016; Wu et al., 2020; Chen et al., 2023; Ge et al., 2024). During a long range transport physicochemical properties of dust particles can significantly be changed by a series of chemical reactions especially in the downwind region of East Asia, where anthropogenic gas pollutants such as O_3, NO_x and NH_3 are abundant (Wang et al., 2014, 2015, 2025; Zhang et al., 2015; Wu et al., 2020).

Since the majority of oxidation products of atmospheric volatile organic compounds (VOCs) are water-soluble, gas-to-particle-phase partitioning of water-soluble organic compounds (WSOCs) is a major formation pathway of SOA in the atmosphere (Ervens et al., 2011; Liu et al., 2012; Gkatzelis et al., 2021; Lv et al., 2022a, b). The gas-to-particle-phase partitioning process is regulated by a variety of factors such as concentrations of VOCs, NH_3 and NO_x and their compositions, in addition to temperature and relative humidity (RH) (Hennigan et al., 2009; El-Sayed et al., 2018). In the past decade, atmospheric environment in East Asia has changed significantly due to sharp reductions in SO_2 and black carbon (BC) emissions in China, which is currently dominated by NO_x, VOCs and NH_3 along with an increasing level of O_3 (Zhang et al., 2020; Li et al., 2021; Liu et al., 2022; Xiao et al., 2022; Wang et al., 2023; Chen et al., 2024). Dust storm from East Asia desert regions is one of the major contributors to the global atmospheric aerosols (Wang et al., 2020). Such reductions in SO_2 and BC in the East Asia atmospheric environment could also significantly alter the physicochemical evolution process of dust particles during long range transport by adsorption and reactions such as gas-to-particles partitioning of WSOCs and SOA formation on the dust particle surface. Therefore, field observations on the gas-to-particle-phase partitioning of WSOCs is necessary for better understanding on SOA formation process in the current East Asia atmosphere.

A few studies have indicated that gas-to-particle phase partitioning of WSOCs in China is much more efficient than that in developed countries such as the United States, mainly due to a high level of NH_3 in China (Zhang et al., 2012; Lv et al., 2022a, b). Our recent observation found that such an enhanced gas-to-particle phase partitioning in China not only increase SOA production but also enhance atmospheric aerosol light absorption (Liu et al., 2023). Up to date, most of field investigations on WSOCs partitioning and organic aerosol light absorption have been conducted in winter with a focus on fine particle pollution (Cheng et al., 2016; Yuan et al., 2020; Lv et al., 2022b; Li et al., 2023a, b; Liu et al., 2024). In contrast, WSOC partitioning behavior and organic aerosol light absorption in East Asia during spring has rarely been investigated, where dust particles and NH_3 in the troposphere are much more abundant in spring than in winter. In this study we performed a simultaneous measurement on the atmospheric gas- and aerosol-phase WSOCs in Shanghai with a focus on the heterogenous formation of SOA on dust surface and its impact on dust particle optical properties. Our work for the first time unveiled that light absorbing ability of Asian dust is remarkably enhanced during long range transport by formation of light absorbing SOA, which is termed as brown carbon, on dust particle surface.

2 Materials and methods

2.1 Samples collection

The filed observation was conducted from 27 March to 21 April 2023 on the campus of East China Normal University (31.03° N, 121.45° E), which is situated on the southern area of Shanghai. All instruments were set on the roof of the Atmospheric Observation Station with the air inlet 10 m above the ground. A modified in-situ gas and aerosol compositions monitor (IGAC, Model 63GA, Fortelice International Co., Ltd., Taiwan, China) was used to synchronously measure gaseous and particulate species with a 3 h interval for WSOCs and a 1 h interval for inorganics ions and small organic acids, respectively (Lv et al., 2022a, b). For the IGAC sampling system, the air was drawn into a $PM_{2.5}$ cyclone inlet and passed through either a wet rotating denuder (gases) or a steam jet aerosol collector (aerosols). The IGAC monitor is coupled with ICS-5000$^+$ ion chromatography (Thermo) and a TOC/TON analyzer (model TOC/TON-L CPH, Shimadzu, Inc., Japan). Due to the difference in the online instrument detection limits, gas-phase WSOC ($WSOC_g$) and particle phase WSOC ($WSOC_p$) and particle-phase water-soluble organic nitrogen (WSON) were measured with a time resolution of 3 h, while inorganic species organic acids were measured with a time resolution of 1 h. In this study, the concentrations of WSON were calculated as the difference between total nitrogen (TN), which was determined by the online TOC/TON analyzer, and total inorganic nitrogen ($IN = NH_4^+ + NO_2^- + NO_3^-$), which was determined by the IGAC-IC, namely, $[WSON] = [TN] - [IN]$. The collection efficiency of IGAC system for both gas- and aerosol-phase species is $> 73\,\%$ (Lv et al., 2022a, b).

$PM_{2.5}$ filter samples were collected on a day/night basis by using a high-volume sampler (1.13 $m^3\,min^{-1}$, TISCH Environmental, Inc.) in the spring of 2023 from 27 March to 21 April 2023 ($N = 50$), while size-segregated aerosols were also collected using an Anderson 9-stage sampler (Thermo Electronic Corporation, USA) at an airflow rate of 28.3 $L\,min^{-1}$ with cutoff points of 0.43, 0.65, 1.1, 2.1, 3.3, 4.7, 5.8 and 9.0 µm, respectively. In this study four sets of the size-resolved aerosol samples were collected with two sets collected in 11–13 April 2023, which is a dust storm period (DS) (see discussion later), while other two sets of the size-resolved aerosol samples were collected in other non-dust storm periods (NDS) (7–10 April). In addition, PM_{10}

samples during a spring dust event of 2023 were also collected in Tengger Desert ($N = 3$), which is one of the major dust source regions in East Asia. Field blanks of each types of samples were also collected every 3–5 d. All of the filter samples were collected onto the pre-baked (450 °C) quartz filters and stored in a freezer (−18 °C) prior to analysis.

Hourly $PM_{2.5}$ and PM_{10} mass concentrations were obtained from the Shanghai Environmental Monitoring Center. The meteorological factors including temperature and RH were monitored by an automatic weather station (MILOS520, Vaisala, Inc., Finland).

2.2 Chemical analysis and light absorption measurement

For the offline-$PM_{2.5}$ samples and 9-stage size-segregated filter samples analysis, a half of each filter sample was cut into pieces and ultrasonically extracted with 45 mL Milli-Q water. The extracts were subsequently filtered with a 0.45 µm syringe filter, and analyzed using ion chromatography (ICS-5000$^+$, Thermo Scientific) for inorganic ions (Na^+, NH_4^+, K^+, Mg^{2+}, Ca^{2+}, Cl^-, NO_2^-, NO_3^-, SO_4^{2-}), organic acids (formic, acetic, oxalic, pyruvic (Pyr) and methanesulfonic acids (MSA). Water-soluble organic (WSOC) and inorganic carbon (WSIC) and WSON of the filter samples were determined by the TOC/TON analyzer above. Meanwhile, optical absorptions of WSOC, i.e., water-soluble brown carbon (BrC), in the size-resolved samples were measured using a liquid waveguide capillary cell UV–Vis spectrometer (LWCC, World Precision Instrument, Inc., USA) coupled with a long effective path length. In our application, light from a light source (DH-Mini, Ocean Optics, Inc., USA) is introduced into the LWCC through a fiber optic cable and, after passing through the LWCC, is collected to the detector (Ocean Optics, Inc., USA). Each instrument was calibrated weekly using authentic standards containing the target compounds. The detection limits of TC, IC and TN were 0.04, 0.05 and 0.01 mg L^{-1}, and other species detection limits were less than 0.01 mL L^{-1}.

Nitroaromatics (NACs) in the filter samples were extracted by a mixture of methanol and dichloromethane (2 : 1, $v : v$), derivatized with N,O-bis-(trimethylsilyl)trifluoroacetamide (BSTFA) and quantified by a gas chromatography (GC, HP7890B) coupled with mass spectroscopy (MS, HP5977B) (Wang et al., 2009). In this study, four NACs were determined, which are 4-nitrophenol (4NP), 2-methoxy-4-nitrophenol (4NGA), 2-methoxy-5-nitrophenol (5NGA), and 5-nitrosalicylicylic acid (5NSA), respectively. For imidiazoles (IMS), an aliquot of the filter samples was extracted with 5 mL of ultrapure water with 1 % ($v : v$) methanol and analyzed using high-performance liquid chromatography (HPLC, Thermo Scientific) coupled with orbitrap-mass spectrometry (MS, Thermo Scientific). A total of eight imidazole compounds (IMs) were quantified in this study, which are 2-mechtlimidazole (2MI), 4(5)-methylimidazole (4MI), 1-ethylimidazole (1EI), 2-ethylimidazole (2EI), 1-phenylimidazole (1PhI), 2-phenylimidazole (2PhI), 2-imidazolcarboxaldehyde (2IC) and 4-imidazolcarboxaldehyde (4IC), respectively. Recoveries of all the detected compounds were better than 85 %. The detailed method for the organic aerosol analysis can be found elsewhere (Li et al., 2020, 2023a; Liu et al., 2023).

2.3 Calculations on aerosol liquid water content and pH of $PM_{2.5}$

Aerosol liquid water content (ALWC) and pH were estimated using the thermodynamic model ISORROPIA-II, based on the hourly measured NH_3, RH, T and $PM_{2.5}$-related chemical compounds. A forward metastable mode was chosen for the calculation (Fountoukis and Nenes, 2007; Song et al., 2018; Wang et al., 2018). Figure S1 in the Supplement compares the concentrations of NH_3 and NO_3^- measured by the IGAC instrument with those predicted by ISORROPIA-II model. As shown in Fig. S1, the predicted are very close to the measured, suggesting that the metastable mode we used can remarkably reproduce the measured and the model results including ALWC and acidity (pH) are reliable. It should be noted that the samples collected under RH > 95 % conditions were excluded in this study, because RH > 95 % conditions could increase ALWC and pH estimation uncertainties.

3 Results and discussion

3.1 Chemical characteristics of different aerosol pollution events

During the campaign $PM_{2.5}$ varied from 3.0 to 87 µg m^{-3} with an average of 30 ± 14 µg m^{-3} (Fig. 1 and Table 1), which is slightly lower than the National Air Quality I Grade Standard of China (35 µg m^{-3}). However, particle pollution with a daily $PM_{2.5} > 35$ µg m^{-3} were frequently observed during the campaign (Fig. 1). In this study, a pollution event lasting for more than two consecutive days with a daily $PM_{2.5}$ levels > 35 µg m^{-3} was defined as a haze episode. As shown in Fig. 1, a dust storm event had occurred in Shanghai from 11 to 13 April with a PM_{10} concentration sharply increased to 986 µg m^{-3}, resulting in the $PM_{2.5}/PM_{10}$ mass ratio down to less than 0.1 and Ca^{2+} up to 2.5 µg m^{-3} (Table 1 and Fig. 1). Thus, here we classified the observation periods of 5–9, 11–13 April as a haze event (HE) and dust storm event (DS), respectively. While those periods with a daily $PM_{2.5} < 35$ µg m^{-3} was defined as a clean period (CP), which occurred from 18–22 April (Fig. 1).

As seen in Table 1, secondary ions (sulfate, nitrate, ammonium, SNA) were the dominant species among the detected components. The mass contribution of SNA to $PM_{2.5}$ reached up to ∼ 69 % in HE, which was 1.6-fold of that in CP, indicating a key role of SNA in the haze formation process. During the DS period, SNA loadings in Shanghai were comparable

Table 1. Meteorological parameters and concentrations of gaseous and particulate pollutants in $PM_{2.5}$ in Shanghai during the spring 2023 campaign.

	Whole campaign	Dust storm	Haze event	Clean period
Meteorological parameters and gaseous pollutants				
RH (%)	59 ± 14	44 ± 18	61 ± 13	63 ± 9
T (°C)	17 ± 4	17 ± 3	13 ± 3	21 ± 3
$WSOC_g^a$ (μgC m^{-3})	8.0 ± 3.4	6.1 ± 1.5	6.0 ± 1.4	8.2 ± 3.3
Major components of $PM_{2.5}$				
$PM_{2.5}$ (μg m^{-3})	30 ± 14	39 ± 16	43 ± 16	20 ± 7
PM_{10} (μg m^{-3})	76 ± 89	301 ± 192	58 ± 15	43 ± 19
$WSOC_p^a$ (μgC m^{-3})	3.1 ± 1.3	2.6 ± 0.7	3.0 ± 0.8	2.8 ± 1.7
NH_4^+ (μg m^{-3})	3.7 ± 2.5	1.3 ± 1.3	6.8 ± 2.1	2.2 ± 0.9
NO_3^- (μg m^{-3})	7.7 ± 6.5	3.2 ± 2.5	15.2 ± 6.2	2.9 ± 1.5
SO_4^{2-} (μg m^{-3})	4.2 ± 2.6	2.1 ± 2.2	6.8 ± 2.9	3.7 ± 1.8
SNA (μg m^{-3})[b]	13.3 ± 11.1	6.5 ± 5.6	25.6 ± 13.1	8.5 ± 3.9
$SNA/PM_{2.5}$ (%)[c]	55 ± 22	16 ± 12	68 ± 13	44 ± 12
Ca^{2+} (μg m^{-3})	0.1 ± 0.2	0.6 ± 0.5	0.08 ± 0.05	0.01 ± 0.01
ALWC[c] (μg m^{-3})[d]	9.6 ± 12.1	2.7 ± 2.2	18.5 ± 14.4	5.3 ± 2.5
pH of $PM_{2.5}$	3.4 ± 0.8	4.8 ± 1.5	3.4 ± 0.3	2.8 ± 0.5
F_p^e	0.28 ± 0.08	0.3 ± 0.06	0.32 ± 0.06	0.24 ± 0.06

[a] $WSOC_g$, is the gas-phase organics while $WSOC_p$, is the organics in $PM_{2.5}$. [b] SNA is the sum of sulfate, nitrate and ammonium. [c] Ratio of sum of NH_4^+, NO_3^- and SO_4^{2-} to $PM_{2.5}$. [d] ALWC: aerosol liquid water content of $PM_{2.5}$. [e] $F_p = \frac{WSOC_p}{WSOC_g + WSOC_p}$.

to that in CP, which only accounted for ∼ 17 % of $PM_{2.5}$. However, the proportion is still remarkably higher than those in Asian desert sources and upwind cities (Table S1), indicating a significant formation of SNA during the dust long-transport (t test, $p < 0.01$). Ca^{2+}, Na^+ and Mg^{2+} were 4–8 times higher in DS than in HE. Such enhancements in metal cations affected the aerosol acidity, resulting in the pH of fine particles ($PM_{2.5}$) rising from 3.3 in non-dust storm period (NDS) to 7.5 in DS (Fig. 1c).

As shown in Table 1, there was a large variability in $WSOC_g$ concentration, which ranged from 0.7 to 19.6 μgC m^{-3} with an average loading of 8.2 ± 3.3 μgC m^{-3} in the CP period and was higher than those in the HE and DS periods (Table 1). The partitioning coefficient of WSOC ($F_p = WSOC_p/(WSOC_p + WSOC_g)$) (0.32 ± 0.06, Table 1) in HE was 33 % higher than that in CP (0.24 ± 0.06, Table 1) and robustly correlated with $WSOC_p$ ($r = 0.68$, $p < 0.01$) (Fig. S2a). A similar strong correlation of $PM_{2.5}$ with $WSOC_p$ was also observed in HE but not in DS (Fig. S2b). Since most components of SOA are water-soluble, such a strong correlation between F_p and $WSOC_p$ suggests that gas-to-particle-phase partitioning of WSOC is a major formation pathway of SOA in the HE period. WSOC level and F_p in DS (0.3 ± 0.06, Table 1) was similar to those in HE and exhibited a well correlation each other ($r = 0.61$, $p < 0.01$) (Fig. S2a), indicating that gas-to-particle partitioning of $WSOC_g$ was also an important formation pathway for SOA in the DS period. As seen in Table 1, SNA accounted for 68 ± 13 % $PM_{2.5}$ in HE but only 16 ± 12 % $PM_{2.5}$ in DS, because $PM_{2.5}$ was dominated by secondary species in HE but by mineral components in DS. Thus, unlike the case in HE, there was no correlation between $PM_{2.5}$ and $WSOC_p$ in DS.

3.2 Factors driving WSOC partitioning during aerosol pollution events

As shown in Table 1 and Fig. 2a, ALWC in HE was 2.5-fold higher than that in CP period and well correlated with F_p ($r = 0.66$, $p < 0.01$), because $PM_{2.5}$ aerosols in the HE period were enriched in hygroscopic SNA, resulting in a high level of ALWC under the humid conditions (Table 1). Thus, ALWC took a key role controlling the partitioning process of WSOC, similar to the results observed during winter in Shanghai, China and Los Angeles and Atlanta, United States (Hennigan et al., 2009; Zhang et al., 2012; Lv et al., 2022b). In contrast, ALWC in the DS period was almost one order of magnitude lower than that in the HE period (Table 1) and did not correlate with F_p (Fig. 2a), because SNA concentrations in the DS period were much lower than those in the HE period (Table 1). Moreover, RH in the DS period was 44 ± 18 % (Table 1), which is higher than the efflorescence RH of SNA but lower than their deliquescence RH and thus not favorable for the formation of aerosol liquid water (Wang et al., 2016, 2025). Therefore,

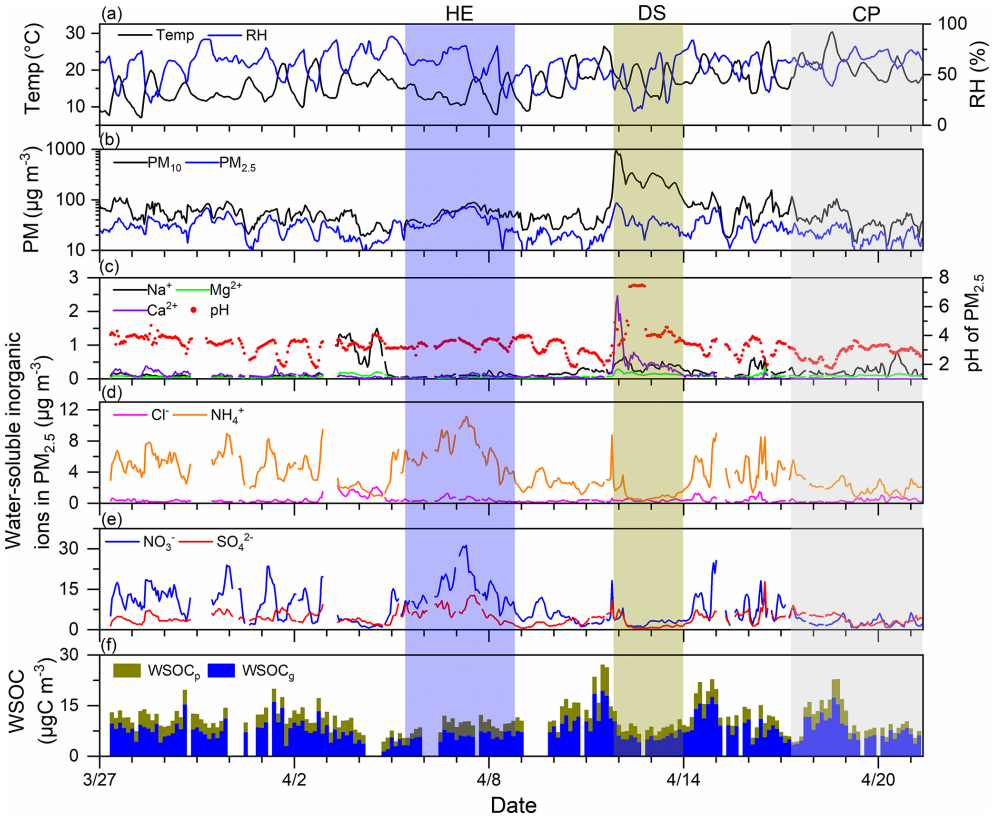

Figure 1. Temporal variations in meteorological parameters and concentrations of major components in $PM_{2.5}$ during the spring of 2023 in Shanghai, China.

WSOC partitioning process during the DS was not regulated by ALWC. In this study, we calculated the contributions of organic matter (OM) and water-soluble inorganic ions to ALWC in the HE period. It can be seen from Fig. S3a, NH_4NO_3 was the largest contributor to ALWC during the haze pollution period, followed by $(NH_4)_2SO_4$ and OM, with the contributions being $56.4 \pm 12.2\,\%$, $29.1 \pm 7.1\,\%$, and $6.1 \pm 3.8\,\%$, respectively. Figure 2b shows that ALWC increased exponentially along with the NH_3-partitioning coefficient ($\varepsilon(NH_4^+) = NH_4^+/(NH_3 + NH_4^+)$) in the HE period and $WSOC_p$ increased in tandem with an increas in ALWC in HE, which increased along with TNH_x concentrations (Fig. 2c). Moreover, as seen in Fig. 2d, $WSOC_p$ well correlated with TNH_x ($= NH_3 + NH_4^+$) in HE ($r = 0.72$, $p < 0.01$), indicating that abundant ammonia in the atmosphere of Shanghai is favorable for WSOC partitioning and SOA formation. Na et al. (2007) and Liu et al. (2021) reported that NH_3 can be neutralized with organic acids to form ammonium salts, thus induce rapid increase in SOA yields. It can be seen from Fig. S3b that particulate carboxylates exponentially increased along with an increase of TNH_x concentration, further demonstrating that NH_3 neutralization with organic acids was also responsible for the strong correlations of TNH_x with F_p in the HE period.

During the DS period, F_p of WSOCs robustly correlated with pH ($r = 0.98$, $p < 0.01$, Fig. 2e), suggesting that pH was a key factor controlling the WSOC partitioning. As we discussed before, ammonia played an important role in $WSOC_p$ formation during the HE period with a strong correlation with TNH_x in HE (Fig. 2d). However, such a correlation was not observed in DS (Fig. 2d), which indicates that ammonia was not an effective factor driving the WSOC partitioning process in the DS period. As shown in Fig. 2f, the sum of Ca^{2+}, Na^+ and Mg^{2+} concentrations showed a significantly correlation with particulate organic acids ($r = 0.88$, $p < 0.01$), including formic, acetic and oxalic acids, during the DS period, because the lower acidity of aerosols in the DS period was favorable for the reactive uptake of acidic organics by dust surface (Table S2).

To further analyze the factors controlling the WSOC partitioning, we investigated the partitioning process of formic and acetic acids, which are abundant species of WSOCs in the atmosphere (Table S2). As shown in Fig. S4, F_p of formic and acetic acids in HE presented strong correlations with ALWC, pH and T. In DS, however, compared with ALWC and T, F_p of formic and acetic acids exhibited a stronger correlation with pH, further indicating that the partitioning of

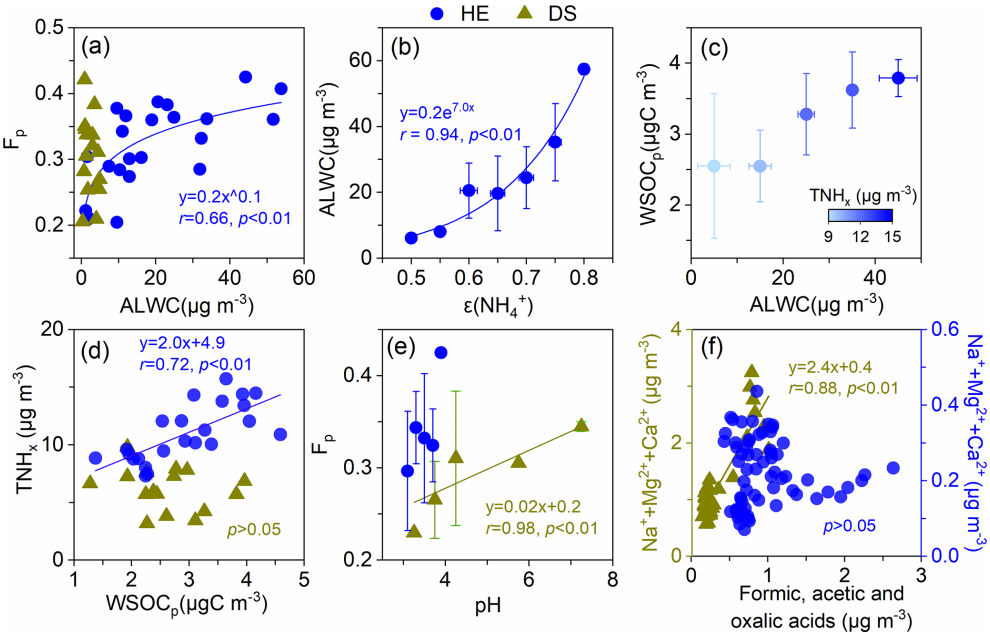

Figure 2. Factors controlling the gas-to-particle phase partitioning of WSOC in haze (HE) and dust storm (DS) events. **(a)** F_p as a function of ALWC in HE and DS. **(b)** ALWC as a function of ammonia partitioning coefficient ($\varepsilon(NH_4^+) = NH_4^+/(NH_3 + NH_4^+)$) in HE. **(c)** Dependence of $WSOC_p$ concentrations on ALWC in HE. **(d)** Linear regression fit for TNH_x versus $WSOC_p$ concentration during HE and DS periods. **(e)** F_p of WSOCs as a function of pH during HE and DS periods. **(f)** Linear regression fit for particulate organic acids and metal cations in HE and DS periods.

WSOC was more significantly affected by the particle acidity in the presence of dust storm.

Apart from the above factors that influence the F_p variations, aerosol mass loading may also affect the partitioning of organic species (Pankow, 1994; Lutz et al., 2019). According to the Raoult's law, the field gas-particle partitioning coefficient can be described as follows (Pankow, 1994):

$$K_i = \frac{i_{\text{particle}}}{i_{\text{gas}}\text{TSP}} \quad \text{(R1)}$$

where K_i is the partitioning constant of i compound, $i_{\text{particle/gas}}$ are the particle and gas phase concentrations of compound i (formic and acetic acids in $PM_{2.5}$ are chosen here), and TSP is the concentration of total suspended particulate material ($PM_{2.5}$ are used here). Figure S5 presents the $i_{\text{particle}}/i_{\text{gas}}$ ratios versus $PM_{2.5}$ for formic and acetic acids during HE and DS periods. Particle/gas ratios of formic and acetic acids did not correlate with $PM_{2.5}$ in both HE and DS periods, indicating that the effect of aerosol mass loading on the uptake of organic acids during the campaign was not significant. As shown in Table 1, the $PM_{2.5}$ loadings in DS were comparable to those in HE, although PM_{10} loading was much higher in the dust storm period. Moreover, the pH (4.8 ± 1.5, Table 1) of $PM_{2.5}$ in DS was 1.4 units higher than that (3.4 ± 0.3) in HE, which means that H^+ concentration in DS was one order of magnitude lower than that in HE. According to the Reactions (R2) and (R3), the low H^+ concentration in DS period was favorable for the organic acid equilibria shifting toward the aerosol aqueous phase. Thus, the impact of pH variation on F_p was much more significant than PM aerosol mass loading in DS, taking a key role in WSOC partitioning process during the DS event.

$$\text{RCOOH(g)} \longleftrightarrow \text{RCOOH(aq)} \quad \text{(R2)}$$

$$\text{RCOOH(aq)} \longleftrightarrow \text{RCOO}^-\text{(aq)} + \text{H}^+\text{(aq)} \quad \text{(R3)}$$

3.3 Gas-to-particle partitioning of WSOC on size-resolved particles

Figure 3 shows the size distributions of water-soluble organic species, including $WSOC_p$, NACs, IMs and $WSON_p$, in the non-dust storm (NDS) and dust storm (DS) periods in Shanghai during the campaign. As shown in Fig. 3a, $WSOC_p$ showed a bimodal size distribution pattern in both periods. The relative abundance of $WSOC_p$ in the coarse mode (> 2.1 μm) accounted for 59 % of the total during the DS period, which is 25 % higher than that in the NDS period. Oxalic, pyruvic and methanesulfonic acids are typical SOA tracers in the atmosphere (Wang et al., 2012, 2015, 2016; Huang et al., 2014; Tang et al., 2019), which displayed a bimodal pattern in the NDS period with two peaks distributing in the fine and coarse modes, respectively (Fig. S6). In contrast, those secondary SOA presented a monomodal size distribution pattern in the DS period with a predominant peak in the coarse mode only. As seen in Table 2, their concentrations are substantially higher than those in the Tengger Desert re-

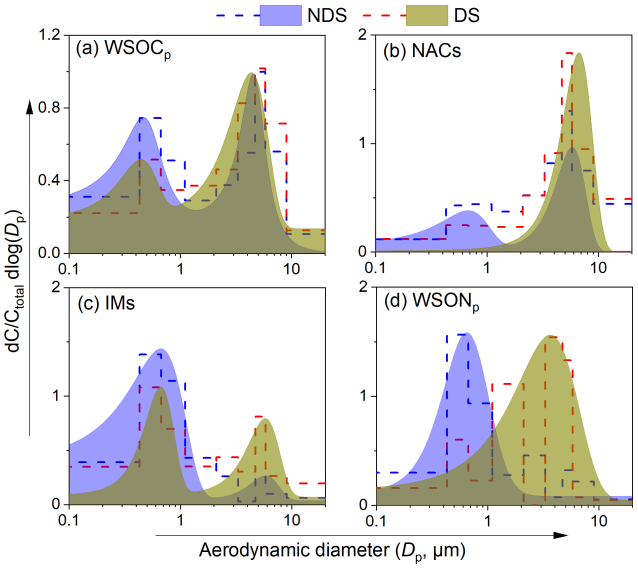

Figure 3. Size distributions of $WSOC_p$, $WSON_p$, nitro-aromatic compounds (NACs) and imidazoles (IMs) in Shanghai during the non-dust storm (NDS) and dust storm (DS) periods. The dashed lines and filled areas are the measured size distribution and fitting results, respectively (C_{total} is the sum of concentration on all the 9-stages).

gion and mostly stayed in the coarse mode (> 2.1 µm) during the DS period, clearly revealing an enhanced SOA formation on the dust particles during their transport from the Asian desert source region to the downwind city. As shown in Fig. S7, F_p of WSOC in the fine and coarse modes were larger than those in the NDS period, especially for the coarse mode of F_p, which was 60 % higher in the DS period than that in the NDS period, indicating that dust surface is favorable for the uptake of $WSOC_g$.

Previous studies reported that NACs can be formed secondarily via both gas-phase and aqueous-phase reaction pathways (Wang et al., 2019; Hems et al., 2020; Ren et al., 2023). For example, benzene reacts with OH radicals and generates phenol. Then, phenol further reacts with NO_2 and yields gaseous nitrophenol (Liang et al., 2020). The latter subsequently partitions to the condensed phase (Lauraguais et al., 2014). Moreover, phenol and catechol can also react with NO_2 radical in the aerosol aqueous phase to form the corresponding NACs (Vione et al., 2004). Our recent study in Shanghai found that the gaseous NACs (i.e., nitrophenol and methylnitrophenols) concentrations were 2 orders of magnitude higher than the particulate ones (Liu et al., 2023). As seen in Fig. 3b, NACs showed a bimodal pattern with a relatively larger peak in the coarse mode during the NDS period. In contrast, NACs almost entirely stayed in the coarse mode during the DS event. Such distinct size distribution patterns indicate that NACs in Shanghai in the DS event were mainly formed by a gas-phase oxidation and subsequent partitioning onto the dust surface.

IMs can be directly emitted from biomass burning process and secondarily produced from reactions of carbonyls with amines and ammonia in aerosol aqueous phase (Lian et al., 2021; Liu et al., 2023). As shown in Fig. 3c, IMs predominantly stayed in the fine mode in the NDS period. However, in the DS period IMs showed a bimodal pattern in the DS period with two equivalent peaks in the fine and coarse modes. respectively. Since IMs were not detected in the Desert source samples (Table 2), the peak of IMs in the coarse particles in Shanghai during the DS period are expected to be secondarily formed on the dust particles via heterogeneous reactions such as the reactions of glyoxal and methylglyoxal with free NH_3 molecules in aerosol aqueous phase (Liu et al., 2023). Size-resolved chemistry analysis results showed that NO_3^- in the coarse mode poorly correlated with NH_4^+ (> 2.1 µm) in the NDS period ($r = 0.29$, $p < 0.05$) but robustly correlated with NH_4^+ ($r = 0.76$, $p < 0.01$) in the DS period (Fig. S8a). Field observations found that NO_3^- in the coarse mode during the NDS period is formed via reaction uptake of gaseous HNO_3 by coarse particles and exists mostly as $Ca(NO_3)_2$ (Tobo et al., 2010; Wu et al., 2020). Therefore, NO_3^- in coarse particles poorly correlates with NH_4^+ (Fig. S8a), because coarse particles are usually enriched with $CaCO_3$, which is more basic than NH_3 (Laskin et al., 2005; Li and Shao, 2009; Tobo et al., 2010). However, in a typical Asian dust storm period the coarse mode of NO_3^- usually strongly correlates with NH_4^+, because there are large amounts of mineral dust particles in Asian dessert region such as Na_2SO_4, $CaSO_4$ and NaCl (Wu et al., 2020). Those mineral dust particles are hygroscopic and can promote the hydrolysis of N_2O_5 on dust particle surface and produce HNO_3, which subsequently neutralize with NH_3 as NH_4NO_3 (Wang et al., 2014; Wu et al., 2020). Therefore, a linear correlation between NO_3^- and NH_4^+ in the coarse mode was observed in Shanghai in DS during the campaign (Fig. S8a). As we discussed in Sect. 3.2, NH_4NO_3 was the biggest contributor to ALWC. Therefore, the formation of hygroscopic species such as NH_4NO_3 can enhance gas-to-particle phase partitioning of $WSOC_g$ and the heterogeneous reactions on the dust surface. Similarly, the coarse mode of oxalic acid robustly and linearly correlated with NH_4^+ in the DS period but not correlated with NH_4^+ in the NDS period ($r = 0.97$, $p < 0.01$) (Fig. S8b), which again suggests an enhanced heterogeneous reaction of SOA on the mineral particle surface during Asian dust long-range transport.

3.4 Enhanced light absorption ability of Asian dust particles

As seen in Fig. 3d, $WSON_p$ presented a monomodal size distribution pattern in Shanghai, peaking at the fine and coarse mode in the NDS and DS periods, respectively. The relative abundance of $WSON_p$ in the coarse mode in the DS period is 0.8 times higher than that in the NDS period. Such an increased $WSON_p$ in the coarse mode in the DS period is in

Table 2. Concentrations of $WSOC_p$, $WSON_p$, organic acids, and inorganic ions and optical properties of $WSOC_p$ in airborne particles in Shanghai and Tengger Desert region.

	Non-dust storm		Dust storm		Tengger Desert
	Fine mode (< 2.1 μm)	Coarse mode (> 2.1 μm)	Fine mode (< 2.1 μm)	Coarse mode (> 2.1 μm)	PM_{10}
$WSOC_p$ (μgC m^{-3})	2.0 ± 0.02	1.8 ± 0.02	2.4 ± 0.01	3.4 ± 0.01	14 ± 7.5
$WSON_p$ (μgN m^{-3})	1.1 ± 0.02	0.3 ± 0.01	0.7 ± 0.01	0.5 ± 0.01	ND[c]
PM (μg m^{-3})	19	48	52	367	402 ± 75
Oxalic acid (μg m^{-3})	0.7 ± 0.04	0.4 ± 0.02	0.3 ± 0.02	1.4 ± 0.1	0.7 ± 0.08
Pyr[a] (μg m^{-3})	0.06 ± 0.01	0.09 ± 0.01	0.03 ± 0.01	0.2 ± 0.01	0.03 ± 0.01
MSA[b] (μg m^{-3})	0.1 ± 0.01	0.1 ± 0.02	0.09 ± 0.01	0.5 ± 0.04	ND[c]
NACs (ng m^{-3})	0.5 ± 0.02	0.9 ± 0.03	0.5 ± 0.01	1.7 ± 0.01	ND[c]
IMs (ng m^{-3})	0.7 ± 0.02	0.1 ± 0.01	0.5 ± 0.02	0.2 ± 0.01	ND[c]
Abs_{365} (M m^{-1})	1.9 ± 0.2	0.8 ± 0.08	2.2 ± 0.2	2.6 ± 0.3	2.5 ± 0.4
MAC_{365} (m^2 g^{-1})	1.0 ± 0.04	0.4 ± 0.02	0.9 ± 0.04	0.8 ± 0.04	0.2 ± 0.09

[a] Pyr: pyruvic acid. [b] MSA: methanesulfonic acid. [c] ND: not detected.

good agreement with that of NACs and IMs and indicates an enhanced formation of nitrogen-containing organic compounds on dust surface (Fig. 3b–d).

Previous researches have shown that many of nitrogen-containing organic compounds in the troposphere are light absorbing brown carbon (BrC) (Laskin et al., 2015, 2025; Liu et al., 2024). Thus, here we further investigate the optical properties of the dust samples. As seen in Table 2, Abs_{365} (1.9 M m^{-1}) and MAC_{365} (1.0 m^2 g^{-1}) of BrC in the fine mode during the NDS period were comparable to those during the DS period (2.2 M m^{-1} and 0.9 m^2 g^{-1}, respectively). However, Abs_{365} and MAC_{365} (2.6 M m^{-1}, 0.8 m^2 g^{-1}, Table 2) in the coarse mode in the DS period were 2–3 times higher those (0.8 M m^{-1}, 0.4 m^2 g^{-1}, Table 2) in the NDS period, respectively, suggesting an enhanced light absorption of coarse particle in the Asian dust storm events. To reveal the nature of such an increase in light absorption of dust particles, we measured the optical properties of atmospheric PM_{10} collected in Tengger Desert. As shown in Fig. 4a, MAC of water-soluble BrC in total suspended particles (TSP) in the wavelength range of $\lambda = 250$–600 nm in Shanghai during the DS period is slightly higher than that in the NDS period, but it is more than two times that in Tengger Desert region, suggesting a remarkable increase in light absorption ability of TSP in the downwind city during both NDS and DS periods. MAC_{365} of BrC in the coarse mode during the DS period in Shanghai (0.8 m^2 g^{-1}, Table 2) is four times that in Tengger Desert regions (0.2 ± 0.09 m^2 g^{-1}, Table 2). As shown in Fig. 4b, $MAC_{250–600}$ of water-soluble BrC in the fine mode during both sampling periods were comparable, but the $MAC_{250–600}$ in the coarse mode during DS period was significantly higher than that in NDS period. Such an increase in light absorption that only occurred in the coarse mode clearly demonstrates that light absorption ability of Asian dust particles in the DS period was significantly strengthened during

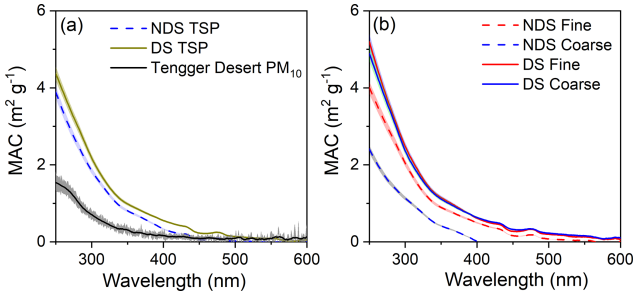

Figure 4. Optical properties of $WSOC_p$ of PM_{10} in Tengger Desert regions and TSP in Shanghai during the dust storm (DS) and non-dust storm (DS) periods. **(a)** Mass absorption coefficient (MAC) of $WSOC_p$. **(b)** MAC of $WSOC_p$ in the fine (< 2.1 μm) and coarse (> 2.1 μm) modes of atmospheric particles in Shanghai.

the long-range transport, which is mostly due to an efficient formation of nitrogen-containing organic compounds on the dust surface.

From Fig. 4b one may further see that the high $MAC_{250–600}$ values at the coarse mode in the DS period largely occurred at the 250–350 nm. As reported by previous studies (Yuan et al., 2020; Liu et al., 2023), light absorption of NACs mainly peaks at a wavelength range large than 350 nm while IMs absorb light mostly at a wavelength less than 300 nm. Thus, here we quantified the contribution of IMs light absorption in the coarse mode during DS period. Based on its concentration and light absorption properties, the light absorption contribution of each individual chromophore to the total BrC in the wavelength range of 250–400 nm was calculated (Text S2). As seen in Fig. 5, IMs show two large absorption peaks at wavelengths of 260 and 290 nm, respectively, which are mainly associated with the absorption of 2 IC and 4 IC. Moreover, it can also be seen

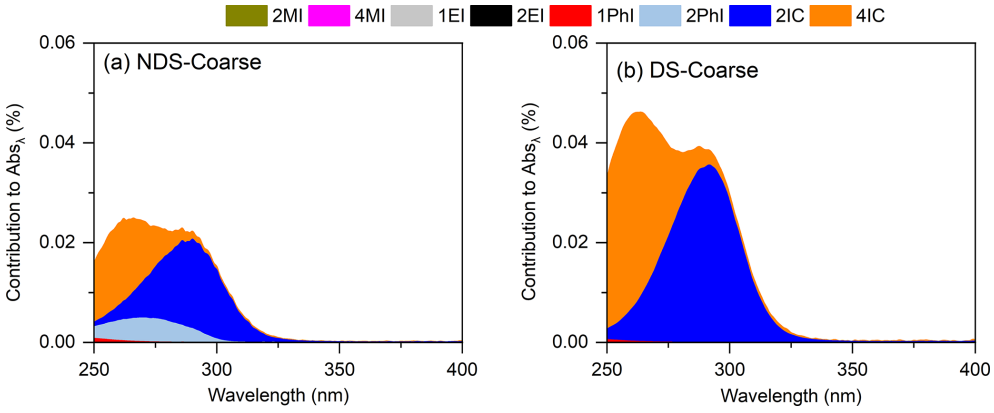

Figure 5. Light absorption contributions of IMs to water-soluble BrC over the wavelength range of 250–400 nm in the coarse mode in NDS and DS periods.

that IMs light absorption contribution to light absorption of water-soluble BrC in DS is almost twice that of NDS, indicating a significant contribution of aqueous phase formation to BrC in DS. This result further suggests that an enhanced heterogeneous formation of nitrogen-containing organics including IMs on the dust particles surface are responsible for the increased light absorbing of Asian dust during a long-range transport.

4 Summary and implications

In this study we synchronously measured the hourly concentrations of gaseous and particulate WSOC in Shanghai, a downwind city of East Asian desert sources, along with measurements on organic tracers and inorganic ions in the gas- and aerosol- phases. We found that the gas-to-aerosol-phase partitioning coefficient (F_p) of WSOC on the dust storm days (0.3 ± 0.06) in the city is comparable to that on the haze days (0.32 ± 0.06), although the meteorological conditions were drier and hotter during the dust storm period and thus not favorable for the WSOC partitioning, suggesting an enhancing effect of dust particles on the SOA formation on the dust particle surface. In this study, we found the F_p variation was influenced by ALWC in HE but by pH in DS. Moreover, $WSOC_p$ and its light absorption at $\lambda_{365\,nm}$ in the coarse mode was increased significantly in DS period than in NDS period. Notably, by comparing with the aerosol optical properties in Tengger desert, we further found that Asian dust aerosols became much more light absorbing with a MAC four times that in the Asian dust source region, which is caused by the enhanced SOA formation on the dust surface during the long-range transport through adsorption and heterogenous formation of light-absorbing brown carbon including nitrogen-containing organics such as nitroaromatics and imidazoles.

Atmospheric NACs and IMs are mostly produced from the reactions of aromatic with NO_x in the gas phase and carbonyls with free NH_3 in the aerosol aqueous phase, respectively (Liu et al., 2023, 2024). Although atmospheric SO_2 level in China has been decreased significantly due to strict emission control, the concentrations of NO_x, VOCs and NH_3 in the country are still very high, resulting in SOA in the country much more light absorbing than those in USA and other developed countries (Hecobian et al., 2010; Liu et al., 2024; Li et al., 2025). Our previous studies found that secondary brown carbon is much more favorably formed under a high pH conditions (Liu et al., 2023; Zhang et al., 2024), because (1) nitrophenols are acidic species and thus easier to be adsorbed onto dust surface, and (2) a high pH condition favors NH_4^+ dissociate into $NH_3 + H^+$ and thus can promote the reaction of carbonyl with NH_3.

Currently, global aerosol model ensemble estimate that the global dust direct radiative effects is about $-0.4\,W\,m^2$ (Kok et al., 2017). However, by using an analysis on the size and abundance of dust aerosols to constrain the global model, Adebiyi and Kok (2020) found that dust aerosols in the atmosphere is coarser than the size estimated by the current global model ensemble and the dust direct radiative effect is $+0.15\,W\,m^2$, which means that dust cause a net warming of the planet. Based the results given by this study, we believe that if the secondary formation of light absorbing brown carbon is accounted for the global direct radiative effect of dust aerosol is possibly more warming.

Data availability. The data including meteorological data, gaseous pollutants, and major chemical components in $PM_{2.5}$ are freely available at https://doi.org/10.5281/zenodo.14883402 (Li, 2025).

Supplement. The supplement related to this article is available online at https://doi.org/10.5194/acp-25-12037-2025-supplement.

Author contributions. GW designed the experiment and supervised the research. ZL, BX, RL and FW collected the samples. ZL, CW, BX, and GW conducted the sample analysis. ZL, BX, CW, RL, and GW performed the data interpretation. ZL, CW and GW wrote the paper. All the authors contributed to the paper with useful scientific discussions.

Competing interests. The contact author has declared that none of the authors has any competing interests.

Disclaimer. Publisher's note: Copernicus Publications remains neutral with regard to jurisdictional claims made in the text, published maps, institutional affiliations, or any other geographical representation in this paper. While Copernicus Publications makes every effort to include appropriate place names, the final responsibility lies with the authors. Also, please note that this paper has not received English language copy-editing. Views expressed in the text are those of the authors and do not necessarily reflect the views of the publisher.

Acknowledgements. This work was funded by the National Key Research and Development Program of China (grant no. 2023YFC3706302) and the National Natural Science Foundation of China (grant nos. 42130704, U23A2030).

Financial support. This research was financially supported by the National Key Research and Development Program of China (grant no. 2023YFC3706302) and the National Natural Science Foundation of China (grant nos. 42130704 and U23A2030).

Review statement. This paper was edited by Alex Lee and reviewed by three anonymous referees.

References

Adebiyi, A. A. and Kok, J. F.: Climate models miss most of the coarse dust in the atmosphere, Sci. Adv., 6, https://doi.org/10.1126/sciadv.aaz9507, 2020.

Chen, Q., Miao, R. Q., Geng, G. N., Shrivastava, M., Dao, X., Xu, B. Y., Sun, J. Q., Zhang, X., Liu, M. Y., Tang, G. G., Tang, Q., Hu, H. W., Huang, R. J., Wang, H., Zheng, Y., Qin, Y., Guo, S., Hu, M., and Zhu, T.: Widespread 2013–2020 decreases and reduction challenges of organic aerosol in China, Nat. Commun., 15, https://doi.org/10.1038/s41467-024-48902-0, 2024.

Chen, S., Zhao, D., Huang, J., He, J., Chen, Y., Chen, J., Bi, H., Lou, G., Du, S., Zhang, Y., and Yang, F.: Mongolia Contributed More than 42 % of the Dust Concentrations in Northern China in March and April 2023, Adv. Atmos. Sci., 40, 1549–1557, https://doi.org/10.1007/s00376-023-3062-1, 2023.

Cheng, Y., He, K. B., Du, Z. Y., Engling, G., Liu, J. M., Ma, Y. L., Zheng, M., and Weber, R. J.: The characteristics of brown carbon aerosol during winter in Beijing, Atmos. Environ., 127, 355–364, https://doi.org/10.1016/j.atmosenv.2015.12.035, 2016.

El-Sayed, M. M. H., Ortiz-Montalvo, D. L., and Hennigan, C. J.: The effects of isoprene and NO_x on secondary organic aerosols formed through reversible and irreversible uptake to aerosol water, Atmos. Chem. Phys., 18, 1171–1184, https://doi.org/10.5194/acp-18-1171-2018, 2018.

Ervens, B., Turpin, B. J., and Weber, R. J.: Secondary organic aerosol formation in cloud droplets and aqueous particles (aqSOA): a review of laboratory, field and model studies, Atmos. Chem. Phys., 11, 11069–11102, https://doi.org/10.5194/acp-11-11069-2011, 2011.

Fountoukis, C. and Nenes, A.: ISORROPIA II: a computationally efficient thermodynamic equilibrium model for K^+-Ca^{2+}-Mg^{2+}-NH_4^+-Na^+-SO_4^{2-}-NO_3^--Cl^--H_2O aerosols, Atmos. Chem. Phys., 7, 4639–4659, https://doi.org/10.5194/acp-7-4639-2007, 2007.

Ge, J., Li, W., Huang, J., Mu, Q., Li, Q., Zhao, Q., Su, J., Xie, Y., Alam, K., Zhu, Z., and Hu, X.: Dust Accelerates the Life Cycle of High Clouds Unveiled Through Strongly-Constrained Meteorology, Geophys. Res. Lett., 51, e2024GL109998, https://doi.org/10.1029/2024GL109998, 2024.

Gkatzelis, G. I., Papanastasiou, D. K., Karydis, V. A., Hohaus, T., Liu, Y., Schmitt, S. H., Schlag, P., Fuchs, H., Novelli, A., Chen, Q., Cheng, X., Broch, S., Dong, H., Holland, F., Li, X., Liu, Y., Ma, X., Reimer, D., Rohrer, F., Shao, M., Tan, Z., Taraborrelli, D., Tillmann, R., Wang, H., Wang, Y., Wu, Y., Wu, Z., Zeng, L., Zheng, J., Hu, M., Lu, K., Hofzumahaus, A., Zhang, Y., Wahner, A., and Kiendler-Scharr, A.: Uptake of Water-soluble Gas-phase Oxidation Products Drives Organic Particulate Pollution in Beijing, Geophys. Res. Lett., 48, e2020GL091351, https://doi.org/10.1029/2020GL091351, 2021.

Hecobian, A., Zhang, X., Zheng, M., Frank, N., Edgerton, E. S., and Weber, R. J.: Water-Soluble Organic Aerosol material and the light-absorption characteristics of aqueous extracts measured over the Southeastern United States, Atmos. Chem. Phys., 10, 5965–5977, https://doi.org/10.5194/acp-10-5965-2010, 2010.

Hems, R. F., Schnitzler, E. G., Bastawrous, M., Soong, R., Simpson, A. J., and Abbatt, J. P. D.: Aqueous Photoreactions of Wood Smoke Brown Carbon, ACS Earth Space Chem., 4, 1149–1160, https://doi.org/10.1021/acsearthspacechem.0c00117, 2020.

Hennigan, C. J., Bergin, M. H., Russell, A. G., Nenes, A., and Weber, R. J.: Gas/particle partitioning of water-soluble organic aerosol in Atlanta, Atmos. Chem. Phys., 9, 3613–3628, https://doi.org/10.5194/acp-9-3613-2009, 2009.

Huang, R.-J., Zhang, Y., Bozzetti, C., Ho, K.-F., Cao, J.-J., Han, Y., Daellenbach, K. R., Slowik, J. G., Platt, S. M., Canonaco, F., Zotter, P., Wolf, R., Pieber, S. M., Bruns, E. A., Crippa, M., Ciarelli, G., Piazzalunga, A., Schwikowski, M., Abbaszade, G., Schnelle-Kreis, J., Zimmermann, R., An, Z., Szidat, S., Baltensperger, U., Haddad, I. E., and Prévôt, A. S. H.: High secondary aerosol contribution to particulate pollution during haze events in China, Nature, 514, 218–222, https://doi.org/10.1038/nature13774, 2014.

Kok, J. F., Ridley, D. A., Zhou, Q., Miller, R. L., Zhao, C., Heald, C. L., Ward, D. S., Albani, S., and Haustein, K.: Smaller desert dust cooling effect estimated from analysis of dust size and abundance, Nat. Geosci., 10, 274–278, https://doi.org/10.1038/Ngeo2912, 2017.

Laskin, A., Laskin, J., and Nizkorodov, S. A.: Chemistry of Atmospheric Brown Carbon, Chem. Rev., 115, 4335–4382, https://doi.org/10.1021/cr5006167, 2015.

Laskin, A., West, C. P., and Hettiyadura, A. P. S.: Molecular insights into the composition, sources, and aging of atmospheric brown carbon, Chem. Soc. Rev., 54, 1583–1612, https://doi.org/10.1039/d3cs00609c, 2025.

Laskin, A., Wietsma, T. W., Krueger, B. J., and Grassian, V. H.: Heterogeneous chemistry of individual mineral dust particles with nitric acid: A combined CCSEM/EDX, ESEM, and ICP-MS study, J. Geophys. Res-Atmos., 110, https://doi.org/10.1029/2004JD005206, 2005.

Lauraguais, A., Coeur-Tourneur, C., Cassez, A., Deboudt, K., Fourmentin, M., and Choël, M.: Atmospheric reactivity of hydroxyl radicals with guaiacol (2-methoxyphenol), a biomass burning emitted compound: Secondary organic aerosol formation and gas-phase oxidation products, Atmos. Environ., 86, 155–163, https://doi.org/10.1016/j.atmosenv.2013.11.074, 2014.

Li, D. P., Wu, C., Zhang, S., Lei, Y. L., Lv, S. J., Du, W., Liu, S. J., Zhang, F., Liu, X. D., Liu, L., Meng, J. J., Wang, Y. S., Gao, J., and Wang, G. H.: Significant coal combustion contribution to water-soluble brown carbon during winter in Xingtai, China: Optical properties and sources, J. Environ. Sci., 124, 892–900, https://doi.org/10.1016/j.jes.2022.02.026, 2023a.

Li, H., Qin, X., Chen, J., Wang, G., Liu, C., Lu, D., Zheng, H., Song, X., Gao, Q., Xu, J., Zhu, Y., Liu, J., Wang, X., Deng, C., and Huang, K.: Continuous Measurement and Molecular Compositions of Atmospheric Water-Soluble Brown Carbon in the Nearshore Marine Boundary Layer of Northern China: Secondary Formation and Influencing Factors, J. Geophys. Res-Atmos., 128, e2023JD038565, https://doi.org/10.1029/2023JD038565, 2023b.

Li, J. J., Li, J., Wang, G. H., Zhang, T., Dai, W. T., Ho, K. F., Wang, Q. Y., Shao, Y., Wu, C., and Li, L.: Molecular characteristics of organic compositions in fresh and aged biomass burning aerosols, Sci. Total Environ., 741, https://doi.org/10.1016/j.scitotenv.2020.140247, 2020.

Li, R., Cui, L., Zhao, Y., Zhou, W., and Fu, H.: Long-term trends of ambient nitrate (NO_3^-) concentrations across China based on ensemble machine-learning models, Earth Syst. Sci. Data, 13, 2147–2163, https://doi.org/10.5194/essd-13-2147-2021, 2021.

Li, W., Shao, L., Shi, Z., Chen, J., Yang, L., Yuan, Q., Yan, C., Zhang, X., Wang, Y., Sun, J., Zhang, Y., Shen, X., Wang, Z., and Wang, W.: Mixing state and hygroscopicity of dust and haze particles before leaving Asian continent, J. Geophys. Res-Atmos., 119, 1044–1059, https://doi.org/10.1002/2013JD021003, 2014.

Li, W. J. and Shao, L. Y.: Observation of nitrate coatings on atmospheric mineral dust particles, Atmos. Chem. Phys., 9, 1863–1871, https://doi.org/10.5194/acp-9-1863-2009, 2009.

Li, Y., Fu, T.-M., Yu, J. Z., Zhang, A., Yu, X., Ye, J., Zhu, L., Shen, H., Wang, C., Yang, X., Tao, S., Chen, Q., Li, Y., Li, L., Che, H., and Heald, C. L.: Nitrogen dominates global atmospheric organic aerosol absorption, Science, 387, 989–995, https://doi.org/10.1126/science.adr4473, 2025.

Li, Z.: Simultaneous measurement on atmospheric gas- and aerosol-phase water-soluble organics during dust storm period: a case study in Shanghai, Zenodo [data set], https://doi.org/10.5281/zenodo.14883402, 2025.

Lian, X., Zhang, G., Yang, Y., Lin, Q., Fu, Y., Jiang, F., Peng, L., Hu, X., Chen, D., Wang, X., Peng, P. A., Sheng, G., and Bi, X.: Evidence for the Formation of Imidazole from Carbonyls and Reduced Nitrogen Species at the Individual Particle Level in the Ambient Atmosphere, Environ. Sci. Tech. Let., 8, 9–15, https://doi.org/10.1021/acs.estlett.0c00722, 2021.

Liang, Y. H., Wang, X. F., Dong, S. W., Liu, Z. Y., Mu, J. S., Lu, C. Y., Zhang, J., Li, M., Xue, L. K., and Wang, W. X.: Size distributions of nitrated phenols in winter at a coastal site in north China and the impacts from primary sources and secondary formation, Chemosphere, 250, https://doi.org/10.1016/j.chemosphere.2020.126256, 2020.

Liu, J., Zhang, X., Parker, E. T., Veres, P. R., Roberts, J. M., de Gouw, J. A., Hayes, P. L., Jimenez, J. L., Murphy, J. G., Ellis, R. A., Huey, L. G., and Weber, R. J.: On the gas-particle partitioning of soluble organic aerosol in two urban atmospheres with contrasting emissions: 2. Gas and particle phase formic acid, J. Geophys. Res-Atmos., 117, https://doi.org/10.1029/2012JD017912, 2012.

Liu, S., Huang, D., Wang, Y., Zhang, S., Liu, X., Wu, C., Du, W., and Wang, G.: Synergetic effects of NH_3 and NO_x on the production and optical absorption of secondary organic aerosol formation from toluene photooxidation, Atmos. Chem. Phys., 21, 17759–17773, https://doi.org/10.5194/acp-21-17759-2021, 2021.

Liu, X., Wang, H., Wang, F., Lv, S., Wu, C., Zhao, Y., Zhang, S., Liu, S., Xu, X., Lei, Y., and Wang, G.: Secondary Formation of Atmospheric Brown Carbon in China Haze: Implication for an Enhancing Role of Ammonia, Environ. Sci. Technol., 57, 11163–11172, https://doi.org/10.1021/acs.est.3c03948, 2023.

Liu, X., Wu, C., Li, Z., Li, R., Wang, F., Lv, S., Li, R., Zhang, F., Wang, H., Liang, C., Zhang, L., and Wang, G.: Atmospheric brown carbon in China haze is dominated by secondary formation, Sci. Total Environ., 945, 173901, https://doi.org/10.1016/j.scitotenv.2024.173901, 2024.

Liu, Y. C., Zhan, J. L., Zheng, F. X., Song, B. Y., Zhang, Y. S., Ma, W., Hua, C. J., Xie, J. L., Bao, X. L., Yan, C., Bianchi, F., Petäjä, T., Ding, A. J., Song, Y., He, H., and Kulmala, M.: Dust emission reduction enhanced gas-to-particle conversion of ammonia in the North China Plain, Nat. Commun., 13, https://doi.org/10.1038/s41467-022-34733-4, 2022.

Lutz, A., Mohr, C., Le Breton, M., Lopez-Hilfiker, F. D., Priestley, M., Thornton, J. A., and Hallquist, M.: Gas to Particle Partitioning of Organic Acids in the Boreal Atmosphere, ACS Earth Space Chem., 3, 1279–1287, https://doi.org/10.1021/acsearthspacechem.9b00041, 2019.

Lv, S. J., Wu, C., Wang, F. L., Liu, X. D., Zhang, S., Chen, Y. B., Zhang, F., Yang, Y., Wang, H. L., Huang, C., Fu, Q. Y., Duan, Y. S., and Wang, G. H.: Nitrate-Enhanced Gas-to-Particle-Phase Partitioning of Water- Soluble Organic Compounds in Chinese Urban Atmosphere: Implications for Secondary Organic Aerosol Formation, Environ. Sci. Tech. Let., 10, 14–20, https://doi.org/10.1021/acs.estlett.2c00894, 2022a.

Lv, S. J., Wang, F. L., Wu, C., Chen, Y. B., Liu, S. J., Zhang, S., Li, D. P., Du, W., Zhang, F., Wang, H. L., Huang, C., Fu, Q. Y., Duan, Y. S., and Wang, G. H.: Gas-to-Aerosol Phase Partitioning of Atmospheric Water-Soluble Organic Compounds at a Rural Site in China: An Enhancing Effect of NH_3 on SOA Formation, Environ. Sci. Technol., 56, 3915–3924, https://doi.org/10.1021/acs.est.1c06855, 2022b.

Na, K., Song, C., Switzer, C., and Cocker, D. R.: Effect of Ammonia on Secondary Organic Aerosol Formation from α-Pinene

Ozonolysis in Dry and Humid Conditions, Environ. Sci. Technol., 41, 6096–6102, https://doi.org/10.1021/es061956y, 2007.

Pankow, J. F.: An absorption model of the gas/aerosol partitioning involved in the formation of secondary organic aerosol, Atmos. Environ., 28, 189–193, https://doi.org/10.1016/1352-2310(94)90094-9, 1994.

Ren, Y., Wang, G., Wei, J., Tao, J., Zhang, Z., and Li, H.: Contributions of primary emissions and secondary formation to nitrated aromatic compounds in themountain background region of Southeast China, Atmos. Chem. Phys., 23, 6835–6848, https://doi.org/10.5194/acp-23-6835-2023, 2023.

Song, S., Gao, M., Xu, W., Shao, J., Shi, G., Wang, S., Wang, Y., Sun, Y., and McElroy, M. B.: Fine-particle pH for Beijing winter haze as inferred from different thermodynamic equilibrium models, Atmos. Chem. Phys., 18, 7423–7438, https://doi.org/10.5194/acp-18-7423-2018, 2018.

Tang, M., Cziczo, D. J., and Grassian, V. H.: Interactions of Water with Mineral Dust Aerosol: Water Adsorption, Hygroscopicity, Cloud Condensation, and Ice Nucleation, Chem. Rev., 116, 4205–4259, https://doi.org/10.1021/acs.chemrev.5b00529, 2016.

Tang, M., Guo, L., Bai, Y., Huang, R.-J., Wu, Z., Wang, Z., Zhang, G., Ding, X., Hu, M., and Wang, X.: Impacts of methanesulfonate on the cloud condensation nucleation activity of sea salt aerosol, Atmos. Environ., 201, 13–17, https://doi.org/10.1016/j.atmosenv.2018.12.034, 2019.

Tobo, Y., Zhang, D., Matsuki, A., and Iwasaka, Y.: Asian dust particles converted into aqueous droplets under remote marine atmospheric conditions, P. Natl. Acad. Sci. USA., 107, 17905–17910, https://doi.org/10.1073/pnas.1008235107, 2010.

Vione, D., Maurino, V., Minero, C., Lucchiari, M., and Pelizzetti, E.: Nitration and hydroxylation of benzene in the presence of nitrite/nitrous acid in aqueous solution, Chemosphere, 56, 1049–1059, https://doi.org/10.1016/j.chemosphere.2004.05.027, 2004.

Wang, G., Zhang, R., Gomez, M. E., Yang, L., Levy Zamora, M., Hu, M., Lin, Y., Peng, J., Guo, S., Meng, J., Li, J., Cheng, C., Hu, T., Ren, Y., Wang, Y., Gao, J., Cao, J., An, Z., Zhou, W., Li, G., Wang, J., Tian, P., Marrero-Ortiz, W., Secrest, J., Du, Z., Zheng, J., Shang, D., Zeng, L., Shao, M., Wang, W., Huang, Y., Wang, Y., Zhu, Y., Li, Y., Hu, J., Pan, B., Cai, L., Cheng, Y., Ji, Y., Zhang, F., Rosenfeld, D., Liss, P. S., Duce, R. A., Kolb, C. E., and Molina, M. J.: Persistent sulfate formation from London Fog to Chinese haze, P. Natl. Acad. Sci. USA, 113, 13630, https://doi.org/10.1073/pnas.1616540113, 2016.

Wang, G., Zhang, F., Peng, J., Duan, L., Ji, Y., Marrero-Ortiz, W., Wang, J., Li, J., Wu, C., Cao, C., Wang, Y., Zheng, J., Secrest, J., Li, Y., Wang, Y., Li, H., Li, N., and Zhang, R.: Particle acidity and sulfate production during severe haze events in China cannot be reliably inferred by assuming a mixture of inorganic salts, Atmos. Chem. Phys., 18, 10123–10132, https://doi.org/10.5194/acp-18-10123-2018, 2018.

Wang, G., Zhang, S., Wu, C., Zhu, T., Xu, X., Ge, S., Sun, H., Sun, Z., Wang, J., Ji, Y., Gao, J., Ren, Y., Li, H., Zhang, F., Wang, Y., and Seinfeld, J. H.: Atmospheric sulfate aerosol formation enhanced by interfacial anions, PNAS Nexus, 4, pgaf058, https://doi.org/10.1093/pnasnexus/pgaf058, 2025.

Wang, G. H., Kawamura, K., and Lee, M.: Comparison of organic compositions in dust storm and normal aerosol samples collected at Gosan, Jeju Island, during spring 2005, Atmos. Environ., 43, 219–227, https://doi.org/10.1016/j.atmosenv.2008.09.046, 2009.

Wang, G. H., Kawamura, K., Cheng, C. L., Li, J. J., Cao, J. J., Zhang, R. J., Zhang, T., Liu, S. X., and Zhao, Z. Z.: Molecular Distribution and Stable Carbon Isotopic Composition of Dicarboxylic Acids, Ketocarboxylic Acids, and α-Dicarbonyls in Size-Resolved Atmospheric Particles From Xi'an City, China, Environ. Sci. Technol., 46, 4783–4791, https://doi.org/10.1021/es204322c, 2012.

Wang, G. H., Cheng, C. L., Huang, Y., Tao, J., Ren, Y. Q., Wu, F., Meng, J. J., Li, J. J., Cheng, Y. T., Cao, J. J., Liu, S. X., Zhang, T., Zhang, R., and Chen, Y. B.: Evolution of aerosol chemistry in Xi'an, inland China, during the dust storm period of 2013 – Part 1: Sources, chemical forms and formation mechanisms of nitrate and sulfate, Atmos. Chem. Phys., 14, 11571–11585, https://doi.org/10.5194/acp-14-11571-2014, 2014.

Wang, G. H., Cheng, C. L., Meng, J. J., Huang, Y., Li, J. J., and Ren, Y. Q.: Field observation on secondary organic aerosols during Asian dust storm periods: Formation mechanism of oxalic acid and related compounds on dust surface, Atmos. Environ., 113, 169–176, https://doi.org/10.1016/j.atmosenv.2015.05.013, 2015.

Wang, H. C., Wang, H. L., Lu, X., Lu, K. D., Zhang, L., Tham, Y. J., Shi, Z. B., Aikin, K., Fan, S. J., Brown, S. S., and Zhang, Y. H.: Increased night-time oxidation over China despite widespread decrease across the globe, Nat. Geosci., 16, https://doi.org/10.1038/s41561-022-01122-x, 2023.

Wang, Y., Hu, M., Wang, Y., Zheng, J., Shang, D., Yang, Y., Liu, Y., Li, X., Tang, R., Zhu, W., Du, Z., Wu, Y., Guo, S., Wu, Z., Lou, S., Hallquist, M., and Yu, J. Z.: The formation of nitro-aromatic compounds under high NO_x and anthropogenic VOC conditions in urban Beijing, China, Atmos. Chem. Phys., 19, 7649–7665, https://doi.org/10.5194/acp-19-7649-2019, 2019.

Wang, Z. L., Huang, X., Wang, N., Xu, J. W., and Ding, A. J.: Aerosol-Radiation Interactions of Dust Storm Deteriorate Particle and Ozone Pollution in East China, J. Geophys. Res-Atmos., 125, https://doi.org/10.1029/2020JD033601, 2020.

Wu, C., Zhang, S., Wang, G. H., Lv, S. J., Li, D. P., Liu, L., Li, J. J., Liu, S. J., Du, W., Meng, J. J., Qiao, L. P., Zhou, M., Huang, C., and Wang, H. L.: Efficient Heterogeneous Formation of Ammonium Nitrate on the Saline Mineral Particle Surface in the Atmosphere of East Asia during Dust Storm Periods, Environ. Sci. Technol., 54, 15622–15630, https://doi.org/10.1021/acs.est.0c04544, 2020.

Xiao, Q. Y., Geng, G. N., Xue, T., Liu, S. G., Cai, C. L., He, K. B., and Zhang, Q.: Tracking $PM_{2.5}$ and O_3 Pollution and the Related Health Burden in China 2013–2020, Environ. Sci. Technol., 56, 6922–6932, https://doi.org/10.1021/acs.est.1c04548, 2022.

Yuan, W., Huang, R.-J., Yang, L., Guo, J., Chen, Z., Duan, J., Wang, T., Ni, H., Han, Y., Li, Y., Chen, Q., Chen, Y., Hoffmann, T., and O'Dowd, C.: Characterization of the light-absorbing properties, chromophore composition and sources of brown carbon aerosol in Xi'an, northwestern China, Atmos. Chem. Phys., 20, 5129–5144, https://doi.org/10.5194/acp-20-5129-2020, 2020.

Zhang, F., Wang, Y., Peng, J. F., Chen, L., Sun, Y. L., Duan, L., Ge, X. L., Li, Y. X., Zhao, J. Y., Liu, C., Zhang, X. C., Zhang, G., Pan, Y. P., Wang, Y. S., Zhang, A. L., Ji, Y. M., Wang, G. H., Hu, M., Molina, M. J., and Zhang, R. Y.: An unexpected catalyst dominates formation and radiative forcing of regional haze, P. Natl. Acad. Sci. USA, 117, 3960–3966, https://doi.org/10.1073/pnas.1919343117, 2020.

Zhang, R., Wang, G., Guo, S., Zamora, M. L., Ying, Q., Lin, Y., Wang, W., Hu, M., and Wang, Y.: Formation of Urban Fine Particulate Matter, Chem. Rev., 115, 3803–3855, https://doi.org/10.1021/acs.chemrev.5b00067, 2015.

Zhang, S., Gao, Y., Xu, X., Chen, L., Wu, C., Li, Z., Li, R., Xiao, B., Liu, X., Li, R., Zhang, F., and Wang, G.: Heterogeneous formation and light absorption of secondary organic aerosols from acetone photochemical reactions: remarkably enhancing effects of seeds and ammonia, Atmos. Chem. Phys., 24, 14177–14190, https://doi.org/10.5194/acp-24-14177-2024, 2024.

Zhang, X., Liu, J., Parker, E. T., Hayes, P. L., Jimenez, J. L., de Gouw, J. A., Flynn, J. H., Grossberg, N., Lefer, B. L., and Weber, R. J.: On the gas-particle partitioning of soluble organic aerosol in two urban atmospheres with contrasting emissions: 1. Bulk water-soluble organic carbon, J. Geophys. Res-Atmos., 117, https://doi.org/10.1029/2012JD017908, 2012.